AD

DEFECT CHARACTERIZATION OF PYROELECTRIC MATERIALS

Final Technical Report
by

David J. Keeble

(11/02)

United States Army

EUROPEAN RESEARCH OFFICE OF THE U.S. ARMY

London, England

CONTRACT NUMBER N68171-99-M-6463

R&D 8828-EE-01

David J. Keeble

UNIVERSITY OF DUNDEE
SCOTLAND
UK

Approved for Public Release; distribution unlimited

REPORT DOCUMENTATION PAGE

Form Approved OMB No. 0704-0188

1. AGENCY USE ONLY (Leave blank)	2. REPORT DATE	3. REPORT TYPE AND DATES COVERED
	November 2002	Final Technical Report

4. TITLE AND SUBTITLE

Defect Characterization of Pyroelectric Materials

5. FUNDING NUMBERS

Contract No. N68171-99-M-6463

6. AUTHOR(S)

David J. Keeble

7. PERFORMING ORGANIZATION NAME(S) AND ADDRESS(ES)

University of Dundee, Scotland, UK

9. SPONSORING/MONITORING AGENCY NAME(S) AND ADDRESS(ES

United States Army, European Research Office of the U.S. Army, London, England

10. SPONSORING/MONITORING AGENCY REPORT NUMBER

R&D 8828-EE-01

11. SUPPLEMENTARY NOTES

Document has 23 references, 8 tables, 16 figures, 28 pages.

12a. DISTRIBUTION/AVAILABILITY STATEMENT

Approved for Public Release; distribution unlimited.

12b. DISTRIBUTION CODE

ABSTRACT (Maximum 200 words)

Two methods for identify point defects applicable to the study of technologically relevant pyroelectric oxide materials have been investigated, namely Positron Annihilation Lifetime Spectroscopy (PALS) and Electron Paramagnetic Resonance (EPR), For this study a PALS spectrometer was constructed. Preliminary PALS and EPR results on powder and ceramic materials are presented.

An operational positron annihilation lifetime spectrometer has been constructed and tested. The resolution function width of approximately 205 ps with a count rate of 130 counts S^{-1} from a 370 kBq^{-1} source was achieved. Two independent analysis algorithms were tested using simulated lifetime spectra. Systematic studies were performed on a series of polycrystalline pure metal samples. This work confirmed the need for accurate source annihilation correction and allowed a methodology to be developed. Further, this procedure allowed the variation in backscatter source contribution with atomic number to be studied.

The spectrometer was then used to study two pyroelectric Pb based perovskite oxide ceramic samples, a La doped PZT sample, $(Pb,La)(Zr,Ti)O_3$, and an undoped $Pb(Sc_{0.5},Ta_{0.5})O_3$ (PST) sample. Fits using maximum entropy method and source corrected fitting using non-linear least square where found to be similar. A second vacancy defect contribution was clearly observed in both samples.

Electron paramagnetic resonance measurements were extended from earlier single crystal $PbTiO_3$ work to powder $Pb(Zr,Ti)O_3$ samples, A series of Mn doped samples was studied. The spectrum was found to contain contributions from both Mn^{4+} and Mn^{2+} charge states.

14. SUBJECT TERMS

Army, Foreign document, Scotland, Positron annihilation, Electron Paramagnetic Resonance, Defects, Impurities, Oxide materials, Pyroelectric materials, Ferroelectric materials

15. NUMBER OF PAGES

16. PRICE CODE

17. SECURITY CLASSIFICATION OF REPORT	18. SECURITY CLASSIFICATION OF THIS PAGE	19. SECURITY CLASSIFICATION OF ABSTRACT	20. LIMITATION OF ABSTRACT
UNCLASSIFIED	UNCLASSIFIED	UNCLASSIFIED	UL

SUMMARY

Two methods for identify point defects applicable to the study of technologically relevant pyroelectric oxide materials have been investigated, namely Positron Annihilation Lifetime Spectroscopy (PALS) and Electron Paramagnetic Resonance (EPR). For this study a PALS spectrometer was constructed. Preliminary PALS and EPR results on powder and ceramic materials are presented.

An operational positron annihilation lifetime spectrometer has been constructed and tested. The resolution function width of approximately 205 ps with a count rate of 130 counts s^{-1} from a 370 kBq^{-1} source was achieved. Two independent analysis algorithms were tested using simulated lifetime spectra. Systematic studies were performed on a series of polycrystalline pure metal samples. This work confirmed the need for accurate source annihilation correction and allowed a methodology to be developed. Further, this procedure allowed the variation in backscatter source contribution with atomic number to be studied.

The spectrometer was then used to study two pyroelectric Pb based perovskite oxide ceramic samples, a La doped PZT sample, $(Pb,La)(Zr,Ti)O_3$, and an undoped $Pb(Sc_{0.5},Ta_{0.5})O_3$ (PST) sample. Fits using maximum entropy method and source corrected fitting using non-linear least square where found to be similar. A second vacancy defect contribution was clearly observed in both samples.

Electron paramagnetic resonance measurements were extended from earlier single crystal $PbTiO_3$ work to powder $Pb(Zr,Ti)O_3$ samples. A series of Mn doped samples was studied. The spectrum was found to contain contributions from both Mn^{4+} and Mn^{2+} charge states.

KEYWORDS

Positron Annihilation, Electron Paramagnetic Resonance, Defects, Impurities, Oxide Materials, Pyroelectric Materials, Ferroelectric Materials.

Table of Contents

Appendixes

Introduction

Development of imaging devices capable of sensitive operation at ambient temperatures and compact and robust enough for the battlefield is a major research and development focus. Devices using pyroelectric materials are have great potential as sensitive infrared (IR) radiation detectors. Optimising the material performance will make an important contribution to device development. There is a need to both maximizing the pyroelectric coefficient, while reducing the dielectric loss, tanδ. The material performance has been observed to depend of $(\varepsilon \tan\delta)^{-1/2}$.[1] Ferroelectric oxide materials have showed the greatest promise. To optimise the device material properties it is necessary to control the microstructure and, in particular, the point defect population.[2] The origin of dielectric loss has been attributed to defects or domain boundaries in imperfect crystals. Charged atomic scale defects such as impurities or vacancy type defects can attract one another forming dipolar defects. It has been found that these result in internal bias fields that can shift and distort the ferroelectric polarization electric field hysteresis loop. Recent first principles calculations suggest the importance of oxygen vacancy metal impurity complexes in ferroelectrics.[3] Defects are able to 'lock' the orientation of the polarization, preventing the full alignment desirable for pyroelectric applications.

Current knowledge on the nature and behaviour of technologically important atomic scale defects in ferroelectric materials lags far behind that in semiconductors. In particular little work has been carried out on $PbTiO_3$ and related materials. There have, however, been some notable recent work in this area.[4-8]

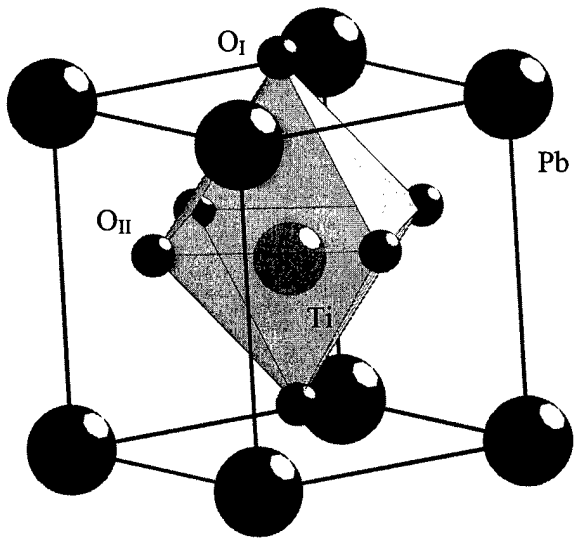

Fig. 1. Crystal structure of $PbTiO_3$.

The crystal structure of these simple perovskite oxides is shown in Fig.1. The structure does not readily accept interstitial defects, impurity ions are found to incorporate by substitution with any required charge compensation occurring by the generation or control of

vacancy defects. However, no unambiguous chemical identification of vacancy defects by atomic scale methods have been made.

The work described here develops two atomic-scale spectroscopy methods with the capability to give unique insight on atomic scale defects in these materials. These are Positron Annihilation methods and Electron Paramagnetic Resonance (EPR) spectroscopy.

Our recent work has shown that positron annihilation methods are sensitive to vacancy defects in these materials and that the Variable Energy Positron Beam (VEPB) method can provide depth profile information on their distribution.[9-14] This work has been carried out as part of a Army Research Laboratory program on ferroelectric materials and infrared detectors. It involved collaboration with members of ARL and with programs at University of Maryland and Brookhaven National Laboratory funded through the ARL Microelectronics Research Collaboration Program (MRCP). The method, VEPB, used so far, however, provides only limited spectroscopy information on the nature of the defects. An alternative positron annihilation technique, positron lifetime spectroscopy, is the primary focus of the work detailed here. The aim of the work has been to develop Positron Annihilation Lifetime Spectroscopy (PALS) methods to compliment VEPB measurements we have made at Brookhaven. PALS allows the contributions from positrons annihilating in the perfect bulk material to be separated form contributions annihilating from vacancy defects. The positron lifetime is a characteristic of particular vacancy defects and can allow the chemical nature of the defect to be identified. Ultimately this new information will contribute to the engineering of the materials and processes to maximize performance.

This report will also briefly address some EPR studies of impurity ions in relevant oxide materials to be used for future positron lifetime experiments.

Introduction to Positron Annihilation

Positron annihilation is particularly sensitive to vacancy related defects in materials. The annihilation characteristics can be obtained from Doppler broadening of the 511keV γ-ray or from a positron lifetime experiment. Both methods allow vacancy-related defects to be identified. Positron lifetime spectroscopy allows the deconvolution of several vacancy-related defect types. The Doppler broadening detection method can be used in conjunction with a variable energy positron beam which allows the positrons to be implanted to specific depths within thin layer samples. In contrast the positron lifetime measurement is confined to bulk samples > 100 μm in thickness. A detailed account of Positron Annihilation Lifetime Spectroscopy will be given in a later section of this report. Here the focus is mainly on the complimentary methods used up to this point.

Positrons implanted in to solids thermalise within 10 ps and enter a Bloch state from which they can annihilate directly or they can be trapped into a localized state from which annihilation can take place on a timescale typically in the range 100 to 500 ps. A thermal positron annihilating with an electron in a solid will do so predominately via a two γ process. These resultant 511 keV annihilation γ-rays, when viewed in the laboratory frame, are Doppler broadened by the longitudinal component of the annihilation pair momentum. The pair momentum is dominated by that of the electron. The Doppler broadened γ-ray energy spectrum provides a measure of the momentum distribution of the electrons with which the positron is annihilating. Vacancy defects, due to the missing ion core, represent an attractive potential to positrons. Annihilation from such a site is more likely to occur with low momentum valance electrons. The Doppler broadened lineshape is characterised by the S-parameter which is defined to be sensitive to low momentum events. It is the number of counts in a narrow window about the centre of the spectrum divided by the total number of

counts in the line, see Fig.2. In addition the electron density at the vacancy is reduced and this results in an increase in the positron lifetime over that for bulk annihilations.

An increase in S-parameter indicates an increase in the concentration of vacancy-related defects and/or an increase in the size of those defects. The technique is sensitive to defect concentrations in the approximate range $10^{15} - 10^{19}$ cm^{-3}, however, this is dependent on the specific positron trapping rate for defects involved. The S-parameter typically increases by 1.5-2.5 % between undefected materials and those with a saturation concentration of monovacancy type defects. The value of the saturation defect S-parameter is a characteristic of the particular defect type and material. A systematic increase in this value with vacancy defect size is observed for any particular material. The variation as a function of defect concentration is modelled for the case of a saturation S value of 1 % is shown in Fig.3.

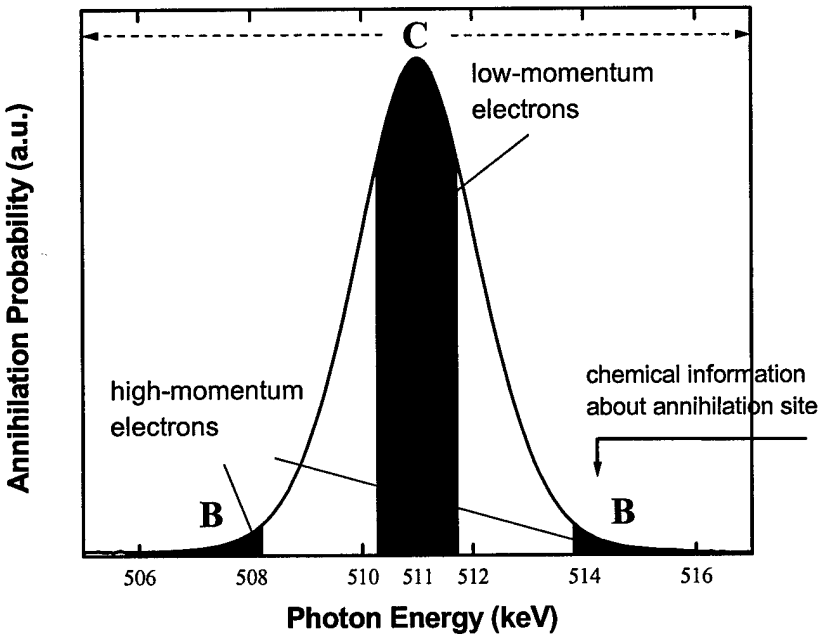

Fig. 2. Doppler Broadened 511 keV gamma-ray energy spectrum. The S parameter is defined as the counts in region A divided by the total counts in the line.

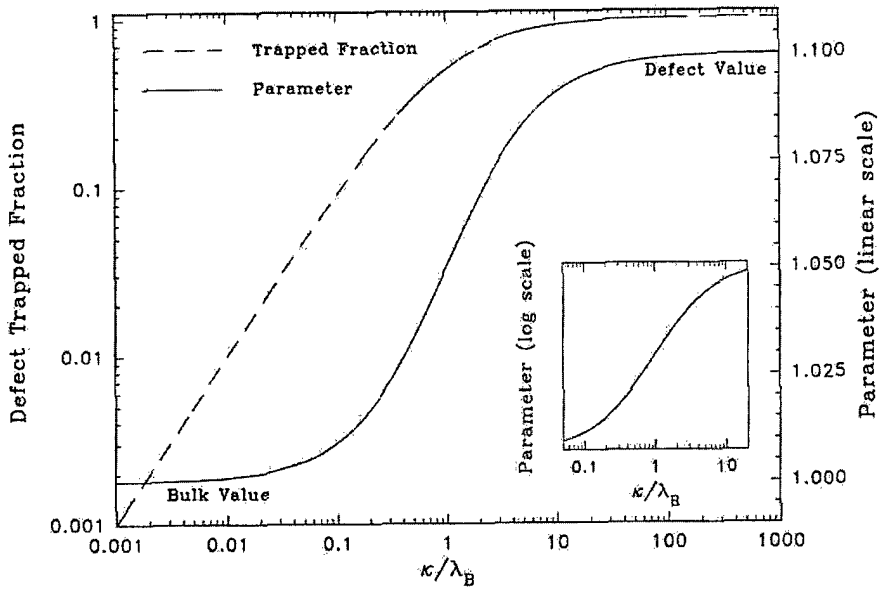

Fig. 3. Positron trapping to a vacancy-related defect as a function of concentration, c_D, with $\kappa = c_D \mu_D$ where μ_D is the defect specific positron trapping rate.

By implanting positrons into a suitable thin metal foil, e.g. tungsten, with a negative workfunction for positrons it is possible to obtain a population of thermal positrons which can then be guided and accelerated to a defined energy. This beam of monoenergetic positrons can then been implanted into a thin film and the mean depth of implantation varied by varying the positron energy. Positron annihilation can then be measured using Doppler broadening, this has the advantage of rapid data collection so allowing depth profiles to be accumulated.

Introduction to EPR

Electron paramagnetic resonance is an established technique capable of detecting paramagnetic defect states with high sensitivity. The limit is approximately 10^{11} paramagnetic centres within the sample under study. For experiments performed on solids using a typical microwave frequency in the 9 GHz band this approximates to defect/impurity concentrations of order 10^{12} cm^{-3}. Paramagnetic centres are impurities or defects that have unpaired electrons, in consequence certain charge states of metal ion impurities or native defects in solids are often paramagnetic. The spectra can be interpreted in terms of a spin-Hamiltonian.

$$H = \beta B \cdot g \cdot S + \Sigma_n \sum_{m=-n}^{m} b_n^m O_n^m + \sum_i \left(I_i \cdot A_i \cdot S - \mu_n g_{n,i} B \cdot I_i \right)$$

The first term is generally the dominant one, it describes the Zeeman interaction between the unpaired spin and the applied magnetic field. The spectroscopy is performed by holding the photon energy constant using a high quality factor microwave resonant cavity and sweeping the external magnetic field so altering the Zeeman splitting of the levels. At resonance microwave power is absorbed by the sample. The ability to resolve interactions with those nuclei composing the local structure of the defect or impurity and that have non-zero nuclear spin give the technique chemical specificity.

Positron Annihilation Lifetime Spectroscopy

Introduction

Positrons are readily available from the radioisotope ^{22}Na, which has the advantages of a relatively long half-life, ~ 2.5 yr, a high yield of positrons and is easily handled in the form of ^{22}NaCl solutions. Crucially for lifetime spectroscopy the emission of a e^+ is accompanied by a 1.27 MeV γ – ray with several picoseconds, see Fig. 4. This birth gamma ray provides a convenient prompt signal for timing experiments.

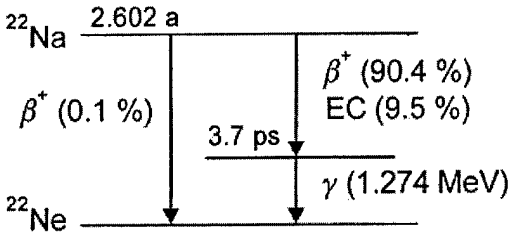

Fig. 4. Radioactive decay of ^{22}Na.

The energy spectrum of the emitted positrons is the conventional β-spectrum with E_{max} = 0.54 MeV. Beam experiments moderate these positrons and in so doing destroy the usefulness of the birth gamma-ray so making lifetime measurements very challenging.

The positron losses energy by core ionisation processes, electron–hole pair production and phonon scattering on a timescale of a few ps. Once at thermal energies the positron can diffuse though the lattice. It is repelled from nuclei, so is more confined to interstitial regions. Semiclassical three-dimensional random-walk theory can describe the diffusion process.

The positron can be considered as entering a delocalised Bloch states. Theses are the only states available in 'perfect' material. However, if open volume defects are present these present a trapping potential for positrons, see Fig. 5.

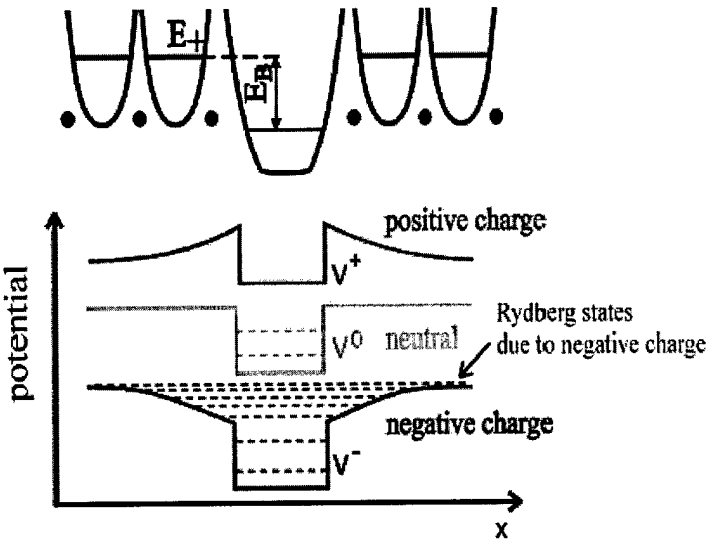

Fig. 5. Positron trapping at vacancy defects.

A localised trapped state can occur at vacancy defects, vacancy clusters, or negative ion defects. Bloch States typically have lifetimes in the 100 – 250 ps range while trapped states at open-volume defects have lifetimes in the 150 – 500 ps range. Positron state lifetimes are much greater than typical thermalisation times. The processes are summarised in Fig. 6.

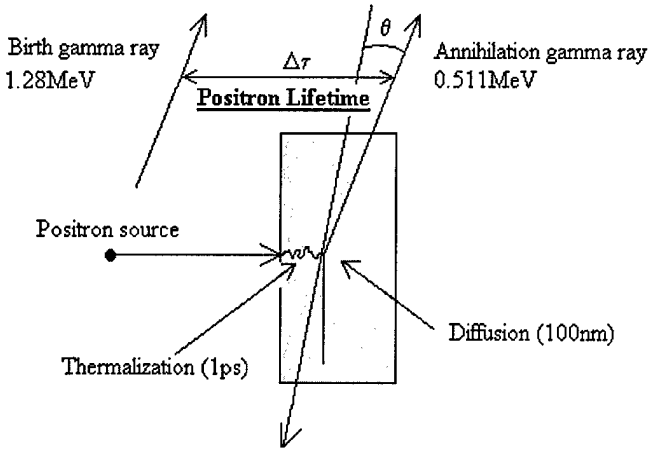

Fig. 6. Schematic of positron implantation and annihilation.

The increase in lifetime at open-volume trap site is due to an a reduction in electron density. The positron lifetime is found to increases with increasing size of open volume, monovacancy < divacancy < 3-vacancy cluster < *etc*. The lifetime can also depend on the charge state of the vacancy.

In the perovskite oxide materials used in infra-red detection applications a commonly expected vacancy defect is a cation vacancy, see Fig. 1, these will have a negative charge state and should be effective positron traps. Oxygen vacancies are also of importance in these materials, however, using a simple ionic model these are expected to be positively charged hence the Coulomb barrier should prevent trapping. Cation vacancy – oxygen vacancy complexes should, however, be positron traps.

A schematic of a positron annihilation lifetime spectrometer is shown in Fig. 7. Two similar detection channels are used, one optimised to detect the 1.27 MeV birth gamma-ray, the second to detect one of the two 0.511 MeV annihilation gamma rays. Both contain a scintillation detector, comprising of a fast photomultiplier tube with a plastic scintillator crystal, feeding a constant fraction discriminator that discriminates the appropriate voltage range of pulses and generates a precise timing output pulse. The timing output pulses are fed to a Time to Amplitude Converter (TAC), which is triggered with the 1.27MeV start channel pulse and stopped by a 0.511 MeV stop channel pulse. The amplitude of the output pulse from the TAC is proportional to START to STOP time interval. These pulses are stored according to amplitude (timing interval) in a Multi-Channel Analyser (MCA).

The sample to be studied is required to be in the form of two, near idenitical, pieces ~ 1cm^2, with thickness > 0.1mm. These are placed each side of the weak, ~370 kBq, ^{22}Na positron source formed by depositing an appropriate amount of ^{22}NaCl solution on a thin foil, *e.g.* 1μm nickel which is folded over to provide a protective layer between the source and the sample. The sample – source package is then mounted between the two scintillation detectors to maximize the capture of emitted gamma-rays.

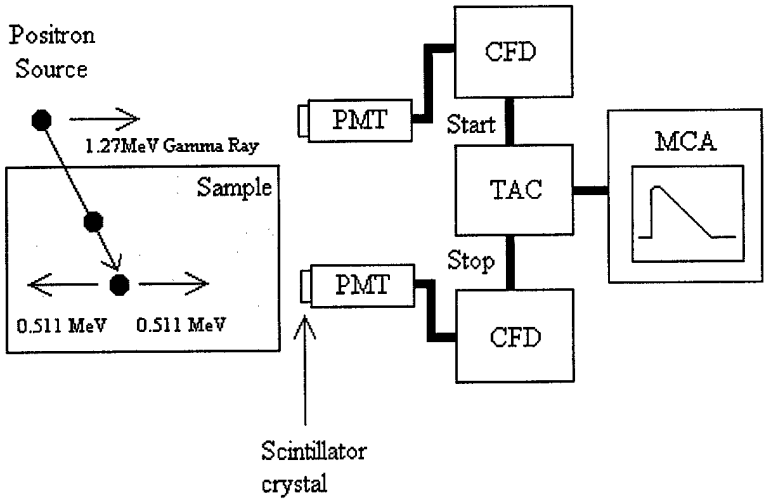

(a) Spectrometer

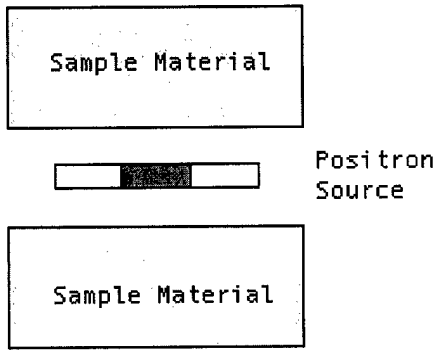

(b) Sample, support-foil, positron source arrangement.

Fig. 7. Schematic of positron lifetime spectrometer.

The resulting MCA timing spectrum contains the experimental positron annihilation spectrum but also contains instrument related contributions. These arise from two main sources. The first is the finite timing resolution function of the whole system. This can be described by up to three Gaussian functions of appropriate widths, positions and intensities. The effective width is typically in the 180 – 250 ps range. The MCA spectrum is a convolution of this instrument timing resolution function and the positron lifetime decay curves. The second instrument contribution adds to the later, positron lifetime components will exist due to positrons that annihilate in the NaCl source crystals and in the thin support foil used to contain the source. These source correction annihilation components must be subtracted from the experimental spectrum to allow the positron annihilation contributions from the sample material to be correctly analysed.

We will return to the practical procedures required for correct analysis of positron lifetime experimental spectra later. First, however, the theory allowing an interpretation of the spectra in terms of trapping centre concentration and type will be outlined.

The theoretical framework used to interpret the positron results is termed the simple trapping model. It will be sufficient for the work described here to outline the simplest version of this model. In this we consider a single positron trap is present in the material, from which the positron is unable to escape once trapped. There are in consequence then two possible positron states, the bulk Bloch state and the defect trapped state, from which the positron can annihilate, see Fig. 8.

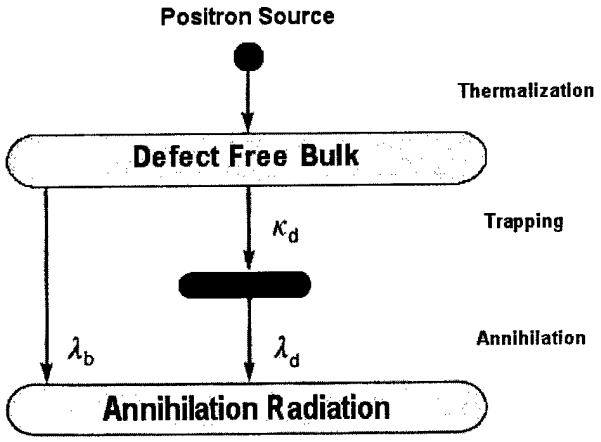

Fig. 8. Simple trapping model

The populations of these states is controlled by the following expressions:-

$$\frac{dn_B}{dt} = -\lambda_B n_B - \kappa n_B \text{ and } \frac{dn_D}{dt} = \kappa n_B - \lambda_D n_D ,$$

where the rate of annihilation from the bulk state is given by λ_B and the annihilation rate at the defect by κ. This model is then equated to the experimental spectrum, which can be described by the expression,

$$-\frac{dn(t)}{dt} = I_1\lambda_1 \exp(-\lambda_1 t) + I_2\lambda_2 \exp(-\lambda_2 t).$$

This spectrum will, in general, comprise of two contributions with lifetimes $\tau_1 = 1/\lambda_1$ and $\tau_2 = 1/\lambda_2$. The relations between the experimental lifetimes/annihilation rates and the model parameters are easily obtained,

$$\kappa = \frac{I_2}{I_1}(\lambda_B - \lambda_D) = I_2(\lambda_1 - \lambda_D) = \frac{\tau_{ave} - \tau_B}{\tau_D - \tau_{ave}}\frac{1}{\tau_B},\ \tau_1 = \frac{1}{\lambda_B + \kappa},\ \tau_2 = \frac{1}{\lambda_D}, \text{ and } \frac{1}{\tau_{bulk}} = \frac{1-I_2}{\tau_1} + \frac{I_2}{\tau_2}.$$

The second lifetime is characteristic of the particular vacancy defect, and the bulk lifetime is the parameter characterising the annihilations from perfect material. The rate of trapping to the vacancy defect population is given by κ. This is related to the concentration of the vacancy defect, c_D, by the expression $\kappa = \mu_D c_D$, where μ_D is a constant termed the defect specific trapping rate. Finally it should be noted that it is often useful to calculate an average positron lifetime, $\tau_{ave} = \sum I_i \tau_i$, where each of the experimentally determined components is

included. This lifetime can give valuable, model independent, information on the trapping behaviour between systematic sets of samples or as a function of temperature or other relevant experimental variables.

In order to apply the above model to the experimental positron lifetime components must be de-convolved from the MCA spectrum. Two independent methods can be used. The most common is to fit a model comprising of an appropriate number of lifetime components along with suitable sum Gaussians functions, *R(t)*, to describe the resolution function,

$$f(t) = R(t) * \sum_{j=1}^{K_0} (A_j \exp(-t/\tau_j) + B)$$

and a number of background counts, *B*, are added. This model is then fitted to the MCA spectrum by a non-linear least-squares method that allows certain parameters to be adjusted, normally these are chosen to be the intensities and values of the lifetime components. The programme RESOLUTION from Riso Laboratories uses this algorithm.

An alternative approach is to define a kernel that includes the

$$K(x, y) = R(t) * A \exp(-t/\tau)$$

and fit this to the MCA spectrum, *Dj*, with the help of an intensity function, Φ_u,

$$\int_a^d K_{j,u} \Phi_u + N_j = D_j$$

using a maximum entropy optimisation. In contrast to the last approach the number of lifetimes in the model is not an input, the output is a lifetime distribution function. The programme MELT from University of Geneva applies this approach.[15]

Experiment

A positron annihilation lifetime spectrometer has been constructed based on a conventional fast-fast coincidence system, see Fig. 7. Two Hamamatsu H2831 photomultiplier tube assemblies with a 6 cm^3 Pilot U crystal for the stop and a 27 cm^3 Bicron 418 crystal for the start were used. Timing pulses come from Ortec 583 constant fraction discriminators into and Ortec 556 time to amplitude converter, the output of which is fed via a Canberra 8075 analogue to digital converter to a FastCom Multi Channel Analyser (MCA). The above are kept in an environment chamber with the temperature controlled to better than ±1 °C with an air-conditioning unit. The resolution function is typically described by three Gaussian functions with widths and intensities of 210 ps at 80 %, 130 ps at 10 %, and 340 ps at 10 %. The count-rate is typically 130 counts s^{-1} from a 370 kBq^{-1} source.

The experimental spectra are fitted using the packages Patfitt-88 and MELT 4.0. As the programs from the Patfitt-88 package run from a DOS command line.[16] A specific programme was written to allow the POSITRON and RESOLUTION programs to be run from a MATLAB environment, which is also used to run the MELT 4.0. The main similarities between the programmes are the definition of the time per channel, the range defining the background, and the resolution function definition. However, there are some parameters specific to MELT 4.0, e.g. entropy weight, cut-off value etc. These can normally be left to their default values for metals and are usually only changed when fitting materials with significantly different lifetimes ranges, e.g. polymers.

Deconvolution of Simulated PALS Spectra

Simulated spectra were generated to test the abilities of both programs and provide a means of comparison. A number of specified lifetime components can be convolved with a resolution function defined by up to five Gaussian functions and a random noise background. The experimental spectra are fitted using the packages Patfitt-88 and MELT 4.0. As the

programs from the Patfitt-88 package run from a DOS command line a specific programme was written to allow the POSITRON and RESOLUTION programs to be run from a MATLAB environment, which is also used to run the MELT 4.0.

The main similarities between the programmes are the definition of the time per channel, the range defining the background, and the resolution function definition. However, there are some parameters specific to MELT 4.0, e.g. entropy weight, cut-off value etc. These can normally be left to their default values for metals and are usually only changed when fitting materials with significantly different lifetimes ranges, e.g. polymers.

Simulated spectra were generated to test the abilities of both programs and provide a means of comparison. A number of specified lifetime components can be convolved with a resolution function defined by up to five Gaussian functions and a random noise background.

A comparison of the ability of the two programmes to resolve two lifetime components has been investigated; Fig. 9 & 10 show the results of both programmes ability to resolve two lifetimes with intensity ratios of 1:1 and 4:1, respectively. As the separation of the lifetimes increases both programs are better able to separate the lifetime components. In the case of MELT the number of lifetimes is determined by programme and not by the user. Only one lifetime is extracted when the lifetime components are close, which is found to be a weighted average. Also seen is the effect of the "lucky" fit using POSITRON when the separations of the lifetimes are less than 10ps. In general it was found that POSITRON can separate two lifetime when $\tau_2=\tau_1*1.5$ and MELT when $\tau_2=\tau_1*1.4$.

Another quantity, which can affect the outcome of either fitting programme is the number of counts present in the spectrum. This has been investigated and the results are shown in Fig. 11. This confirms the accepted believe that more than 3 $x10^6$ counts must be accumulated for a successful analysis.

Particular to MELT is the definition of the quantity T_0. This is the position of the central Gaussian with respect to the closest integer channel position 'to the left'. For instance if the peak channel is 100.7 MELT defines a T_0 of 0.7. The program does have the ability to determine the integer part of the displacement of the main Gaussian. However the fractional part is input by the user with the other Gaussians defined relative to this value. It is typical to use the value of the T_0 obtained from RESOLUTION to begin with. Better fits can be obtained by altering T_0. Fig. 11(a) shows that the use of the fractional time - zero channel number from RESOLUTION to define the fractional part of T_0, results in almost identical results obtain from both programmes. The use of an optimised T_0 does improve the variance of the MELT fits as shown in Fig. 12. Fig 11(b) shows that the lifetimes obtained from the programmes when optimised T_0's are used in MELT, are in slightly poorer agreement. However, the degree of separation is within error values supplied by each programmes and decreases with the number of counts in the spectrum.

Finally Fig. 13 shows the effect of the number of counts in the spectrum on the T_0 values showing that the values obtained from RESOLUTION and from optimization become closer with increasing counts.

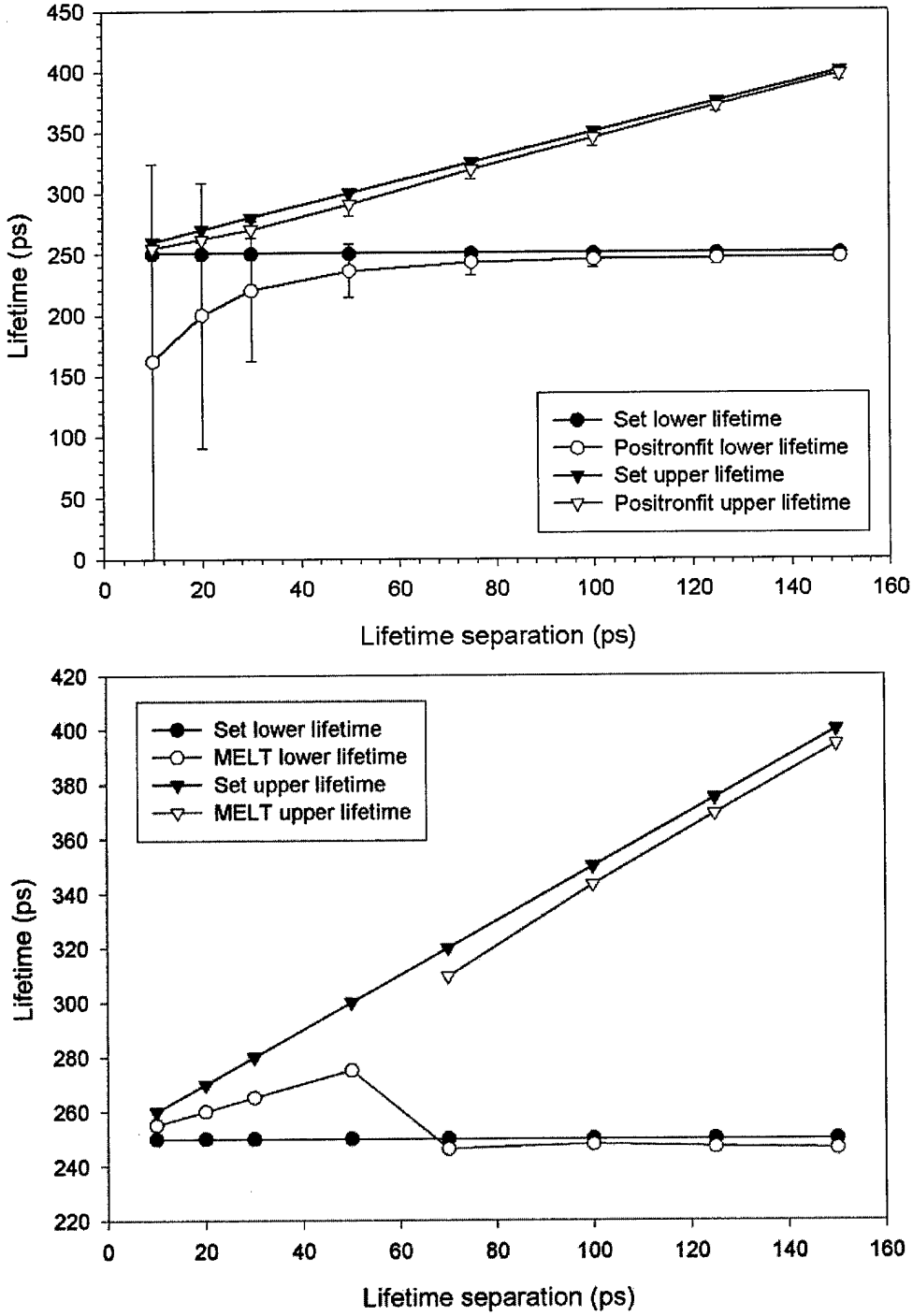

FIGURE 9 – (a) POSITRON and (b) MELT fits using simulated spectra with two lifetime components, intensity ratio 1:1.

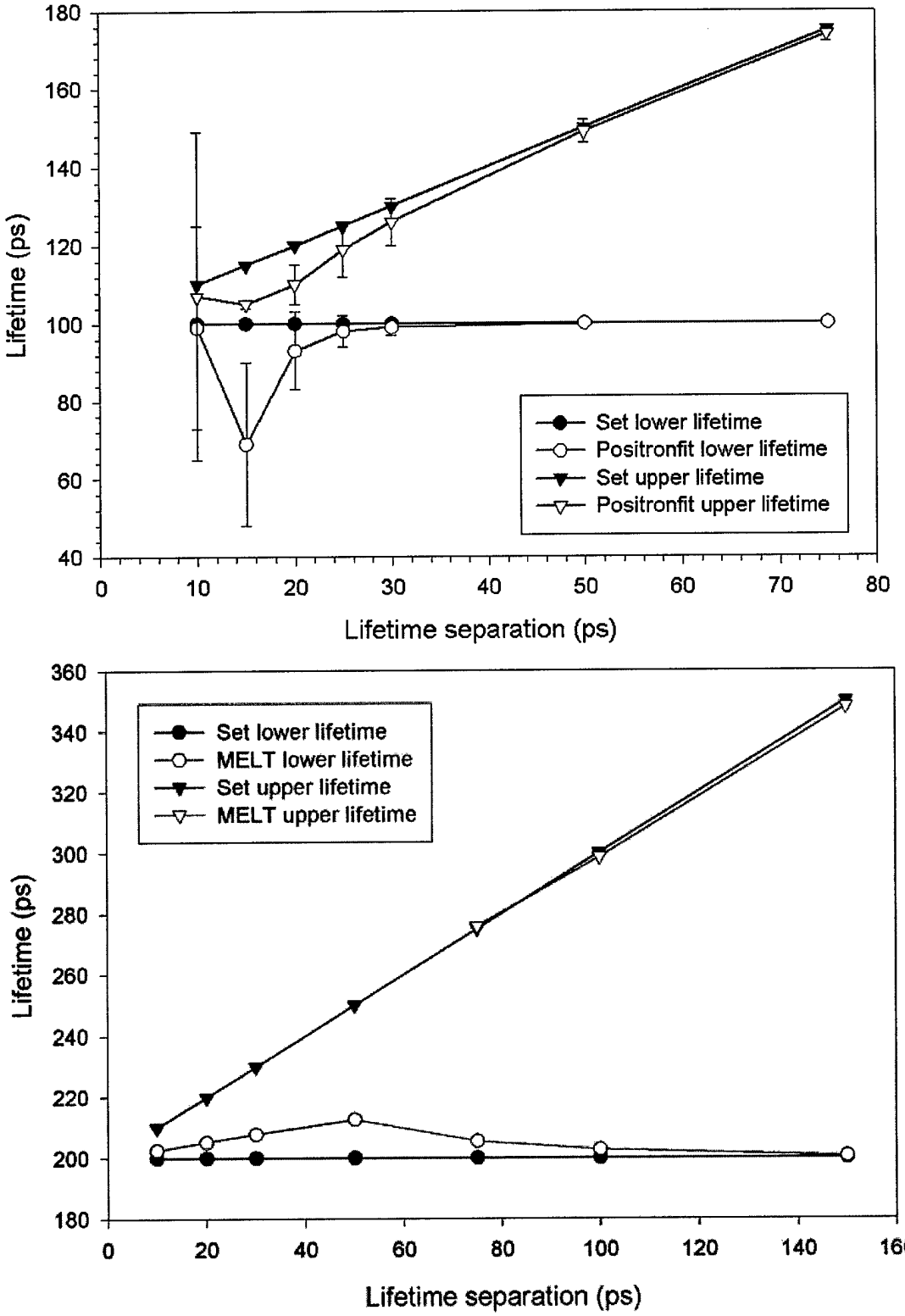

FIGURE 10 – (a) POSITRON and (b) MELT fits using simulated spectra with two lifetime components, intensity ratio 4:1.

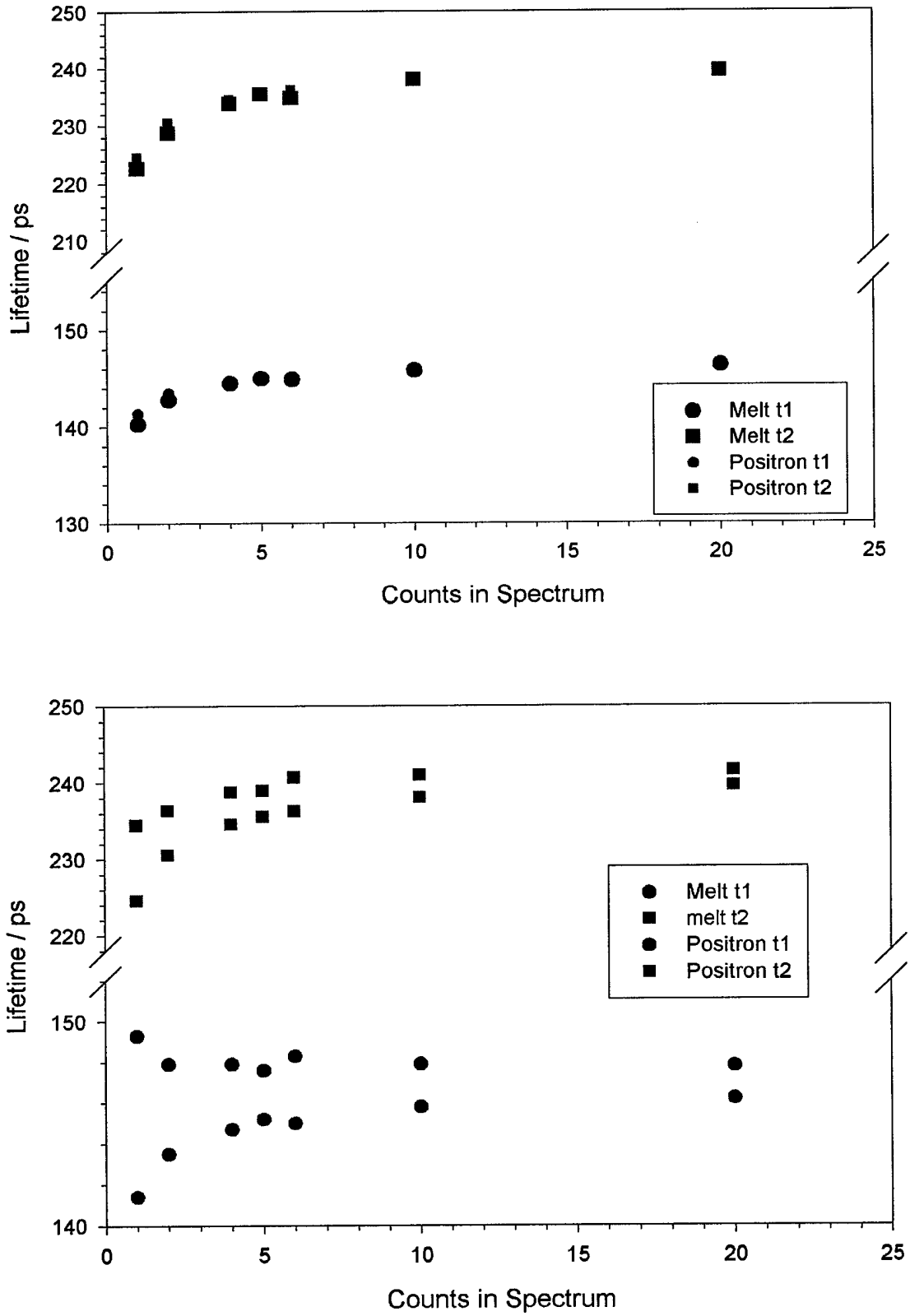

FIGURE 11 – Spectrum with τ_1 = 147ps and τ_1 = 240ps, $I_1 = 4I_2$. POSITRON and MELT fits using T_o from (a) RESOLUION (b) optimized T_o.

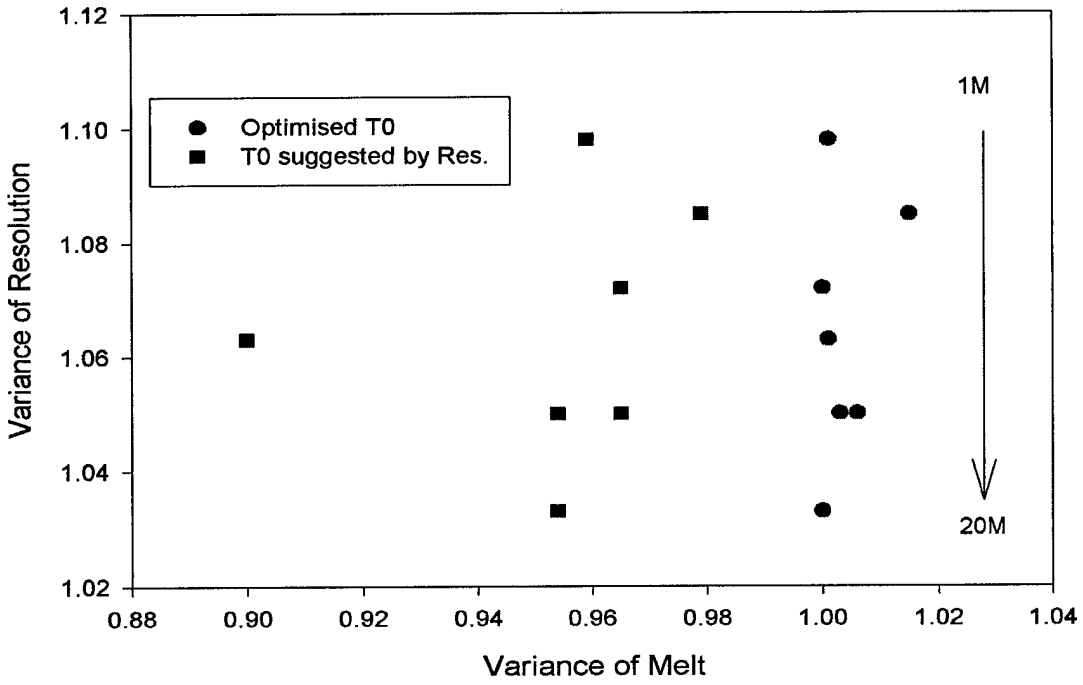

FIGURE 12 – Variance of the MELT and POSITRON fits with optimized T_o and suggested T_o.

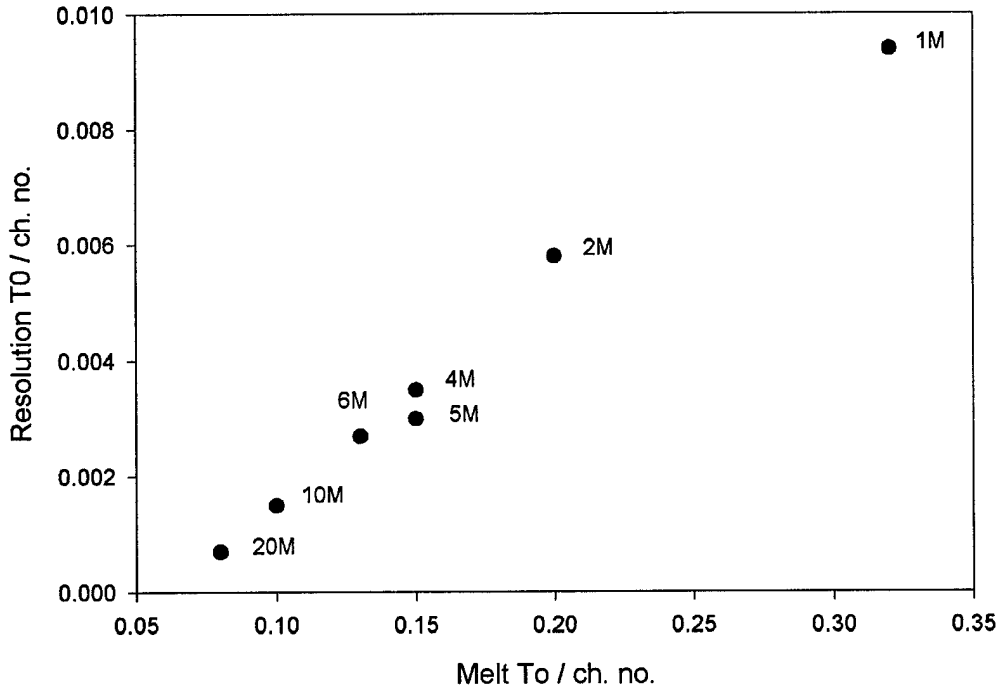

FIGURE 13 – Effect of the number of counts in the lifetime spectrum on T_o from RESOLUTION and optimized T_o used in MELT analysis

PALS Study of Polycrystalline Pure Metals (System test and source correction)

This section describes the testing of the constructed positron lifetime spectrometer. PALS measurements were made on a series of thick polycrystalline metal foil samples. A further aim of this work was to develop a methodology to allow the experimental spectra to be corrected for annihilations occurring in the positron source and the support.

PALS measurements are performed using ^{22}NaCl deposited on metal or polymer foils with a thickness of order 1 – 10 μm. However, although most positrons pass into the material under study there is still a finite probability that some positrons will annihilate in the source foil and salt crystals. Positrons can be reflected from the sample under study back though the source. This backscattering of positrons has been shown to scale with the atomic number of the sample material. The fraction of positrons which annihilate in the source are given by the expression,

$$I_{foil}(z) = 1 - \frac{(1-R_d)I(z)}{1-R_d I(2z)} \tag{0.1}$$

where R_d is the backscatter coefficient of the sample material and I(z) the transmitted intensity. The transmitted intensity can be modeled using

$$I(z) = \exp(-\alpha z) \tag{0.2}$$

where α (cm^{-1}) is the absorption coefficient, given by

$$\frac{\alpha}{\rho} = (30.0 \pm 1.3) Z_{sample}^{0.07} Z_{sourcefoil}^{0.088} [cm^2 g^{-1}]. \tag{0.3}$$

An alternative to (0.2) has also been proposed were an additional exponential integral terms is added, this, however, only makes a significant contribution for very small z values.

$$I(z) = \exp(-\alpha z) + \alpha z Ei(-\alpha z). \tag{0.4}$$

In this work readily available commercial thick metals have been studied using both RESOLUTION/POSITRON and MELT. A summary of previous experimental measurements on the metals studied, Al, Ti, Ni, Ta, and Pb, is given in Table I. Theoretical values have also been included. The metal samples and source foils were obtained from Goodfellow Cambridge Ltd. A summary of the metal samples studied is given in Table II. The positron sources used for these measurements are detailed in Table III. It should be noted that the Al sample had been vacuum annealed for 2 hr at 550°C.

TABLE I – Experimental and Theoretical Metal Positron Lifetimes

Metal	Bulk, τ_B, (ps)	Monovacancy, τ_V, (ps)	References
Al	160(exp), 165 (the)	240(exp), 250 (the)	[17] [18]
Ti	147(exp), 148 (the)	257(exp), 237 (the)	[19] [20]
Ni	102(exp), 96 (the)	142(exp), 180 (the)	[21], [19] [22],[21]
Ta	116(exp), 117 (the)	150-200(exp)	[19] [22],
Pb	200(exp), 187 (the)	281(exp)	[21], [22],

TABLE II – Sample Descriptions

Metal	Treatment	Purity(%)	d(mm)	Z	ρ(g cm^{-3})	Part No.
Al	As rolled	99.99	0.5	13	2.70	AL000650
Ti	Annealed	99.6+	0.5	22	4.5	TI000420
Ni	Annealed	99.98	0.5	28	8.9	NI000590
Ta	Annealed	99.9	0.5	73	16.6	TA000480
Pb	As rolled	99.99	0.55	82	11.35	PB000430
Kapton	UPILEX		0.25	~4	1.42	IM301460

TABLE III – Positron Sources

Support	*d (μm)*	*ρ (g cm^{-3})*	*Part No.*	*Source No.*	*Strength (MBq)*
Al	2	2.70	AL000300	Al-2	0.36
Ni	1	4.5	NI000110	Ni-1	0.43
Kapton	8	1.42	IM301080	Ka-8	0.40

By also including measurements on Kapton it was found possible to estimate the contribution made by annihilations within the source NaCl and, in the case of a Ni contained source, to perform a complete source correction. The validity of (0.2) and (0.4) was tested using the experimental estimates of the intensity of Ni source foil annihilations.

No Source Correction The results from the metals studied with no source correction applied are shown in Table IV, results from Kapton are also included. Fig. 14 shows the average lifetime values obtained for the metal samples.

The MELT and POSITRON fits of the experimental spectra shown in Table IV normally exhibit a third component. This could be attributed to

- positrons annihilating within the source. In the NaCl and from surfaces, or
- annihilations from larger volume defects in the materials.

That source related annihilations are contributing to the spectrum is also clearly shown in Fig. 14 by the systematic increase in the average lifetime when changing the source foil type from Ni to Al to Kapton.

To further investigate the source annihilation contributions fits were carried out using POSITRON only as this allows source correction terms to be readily included.

TABLE IV – PALS results without source correction

Metal	*Source*	*1st Lifetime (MELT / RESOLUTION)*	*2nd Lifetime*	*3rd Lifetime*	χ^2
Al As rolled	Al-2	147(5) ps 80(5) %, 150(3) ps 88(3) %	252(10) ps 19(5) %, 287(10) ps 11(2) %	679(10)ps 0.2(0.2)%,	1.094, 1.10
	Ni-1	148(2) ps 84(1) %, 153(6) ps 91(2) %	268(6) ps 15(1) %, 303(7) ps 8(5) %		1.028, 1.08
	Ka-8	151(5) ps 74(3) %, 146(3) ps 79(5) %	298(9) ps 20(1) %, 313(12) ps 19(4) %	528(10) ps 3(2) %, 740(61) ps 0.7(0.2) %	1.085, 1.08
Ti Annealed	Al-2	125(2) ps 49(2) %, 124(8) ps 46(4) %	246(7) ps 49(2) %, 241(9) ps 50(3) %	493(10)ps 2(1)%, 469(48) ps 2(1) %	1.085, 1.11
	Ni-1	125(2) ps 50(2) %, 130(6) ps 50(4) %	244(8) ps 48(2) %, 246(9) ps 47(3) %	479(9)ps 2(1)%, 511(57) ps 1.5(0.8) %	1.017, 1.06
	Ka-8	127(4) ps 45(3) %, 139(5) ps 52(3) %	260(8) ps 48(2) %, 284(9) ps 45(2) %	465(10) ps 7(3) %, 578(46) ps 2.5(0.8) %	1.008, 1.11
Ni Annealed	Al-2	101(2) ps 84(1) %, 103(3) ps 85(1) %	221(7) ps 14(1) %, 234(12) ps 13(2) %	451(10)ps 2(1)%, 557(64) ps 0.7(0.3) %	1.068, 1.03
	Ni-1	101(2) ps 84(2) %, 105(3) ps 87(2) %	215(4) ps 14(1) %, 235(15) ps 12(2) %	471(15)ps 1.1(0.4)%, 555(71) ps 0.6(0.3) %	1.027, 1.08
	Ka-8	102(2) ps 78(1) %, 104(3) ps 80(1) %	261(10) ps 20(2) %, 288(21) ps 16(1) %	444(10) ps 7(2) %, 490(36) ps 4.5(2) %	1.125, 1.22
Ta Annealed	Al-2	134(2) ps 69(3) %, 139(5) ps 74(5) %	223(4) ps 31(3) %, 236 (11) ps 25(5) %	654(10)ps 0.6(0.2)%, 810(5) ps 0.4(0.1) %	1.115, 1.16
	Ni-1	136(5) ps 72(2) %, 139(5) ps 76(6) %	220(8) ps 27(4) %, 230(13) ps 23(6) %	575(13)ps 0.8(0.2)%, 708(71) ps 0.5(0.2 %	1.053, 1.2
	Ka-8	140(5) ps 68(5) %, 149(2) ps 76(1) %	271(13) ps 24(4) %, 346(9) ps 22(1) %	463(10) ps 7(3) %, 857(116) ps 0.6(0.3) %	1.012, 1.06
Pb As rolled	Al-2	190(3) ps 84(2) %, 170(9) ps 61(8) %	309(5) ps 15(1) %, 270(12) ps 38(8) %	441(13)ps 1.5(0.6)%, 960(144) ps 0.3(0.1) %	1.097, 1.16
	Ni-1	184 (4) ps 80(3) %, 175(8) ps 70(9) %	301 (10) ps 20(4) %, 276(19) ps 29(9) %	1070(24)ps 0.1(0.1)%, 493(80) ps 1(0.7) %	1.087, 0.97
	Ka-8	198(6) ps 77(1) %, 190(4) ps 71(3) %	379 (8) ps 23(1.1) %, 358(9) ps 27(8) %	1767(30) ps 0.1(0.1) %, 477(41) ps 5(3) %	1.098, 1.07
Kapton	Al-2	284(6) ps 38(10) %, 268(11) ps 34(4) %	405(8) ps 61(10) %, 404(4) ps 65(4) %		1.11, 1.06
	Ni-1	266 (4) ps 38(4) %, 239(8) ps 30(9) %	405 (7) ps 62(4) %, 398(19) ps 70(9) %		1.08, 1.08
	Ka-8	318(6) ps 62(5) %, 310(4) ps 60(3) %	438(13) ps 37(6) %, 439(9) ps 40(8) %		1.08, 1.07

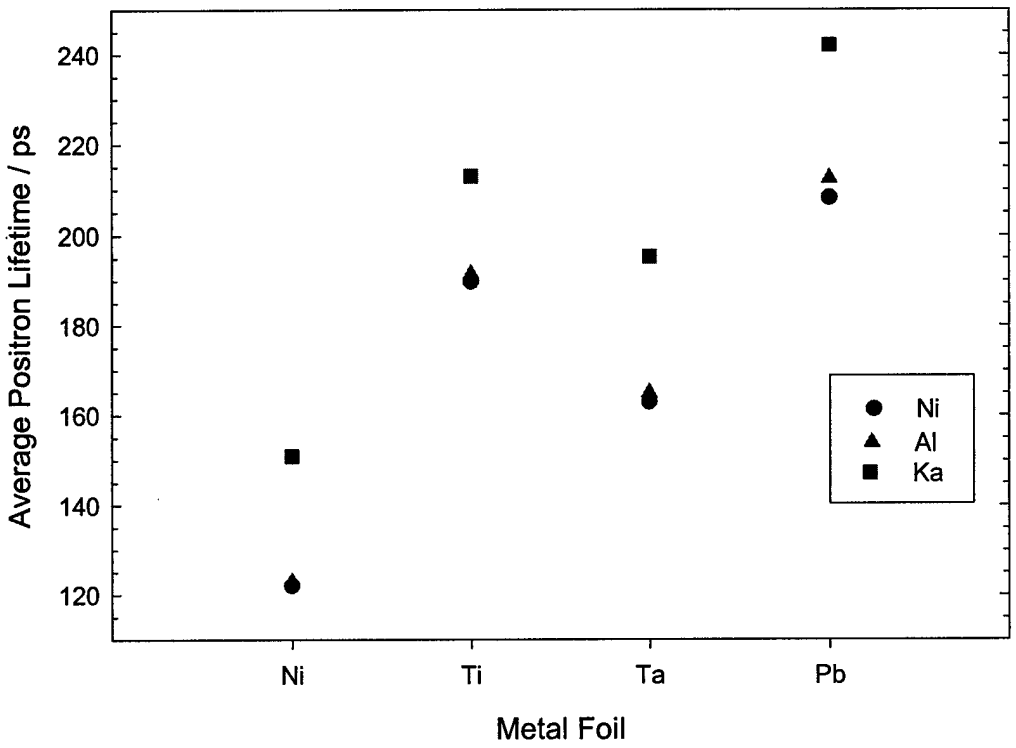

FIGURE 14 – Average lifetime using all components from Table III for the three positron sources used.

A MATLAB programme was written to allow input files to be generated and run where the intensity and lifetime of a component were systematically varied over the ranges 350 – 450 ps and 1 – 10 %. The method was applied to the spectra from each metal studied taken with both the Ni and the Al positron sources. The best χ^2 fits obtained are shown in Fig. 15. All the fits for all metal foils produced the same salt lifetime of ~ (430±10)ps, consistent with previous reported lifetimes. [23]

As expected, backing with dense materials results in an increasing the number of reflections and therefore annihilations occurring within the salt, increasing its intensity contribution. The Ti and Ta points in Fig. 14 suggest a deviation from the general trend. Both exhibit high intensity second lifetime components when compared to the rest. The same approach used to determine the foil lifetime and intensities. This allowed the Ni source (Ni-1) foil lifetime to be estimated to be in the range 110 – 120 ps and that for the aluminum source (Al-2) to be 230 – 240 ps. Determining the intensity values was more difficult. It was not possible to use the procedure for Al-2, however, values were obtained for Ni-1 with number of the elements studied, see Fig. 16. Also shown in the figure are the calculated values from (0.1) using both the exponential model, model 1, and the modified exponential, model 2. The experimental values are in good agreement with the simple exponential model.

Using the values obtained above it was possible to apply source correction in the fitting process using POSITRON. The results for the data collected using source Ni-1 but only applying a NaCl correction are shown in Table V. Applying both a NaCl and a foil correction for the Ni-1 spectra gave the results shown in Table VI. In both cases acceptable variances could only be obtained using two-term fits.

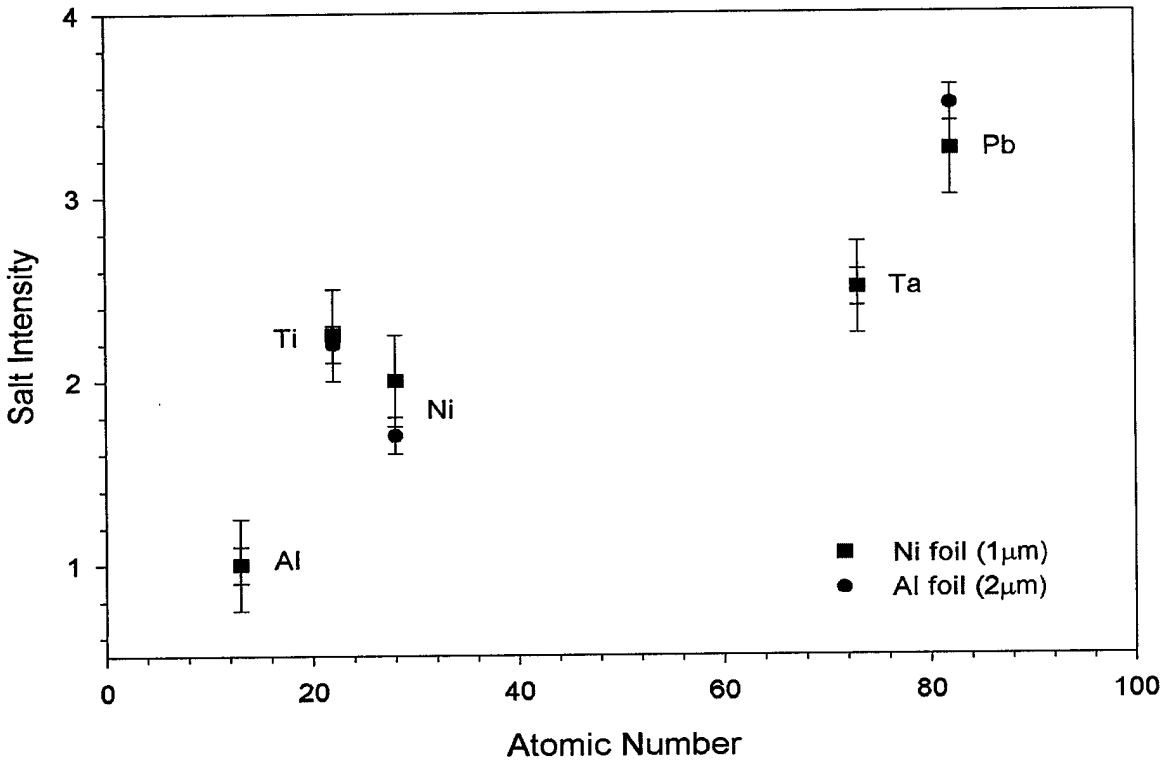

FIGURE 15 – Salt component intensity with various backing materials

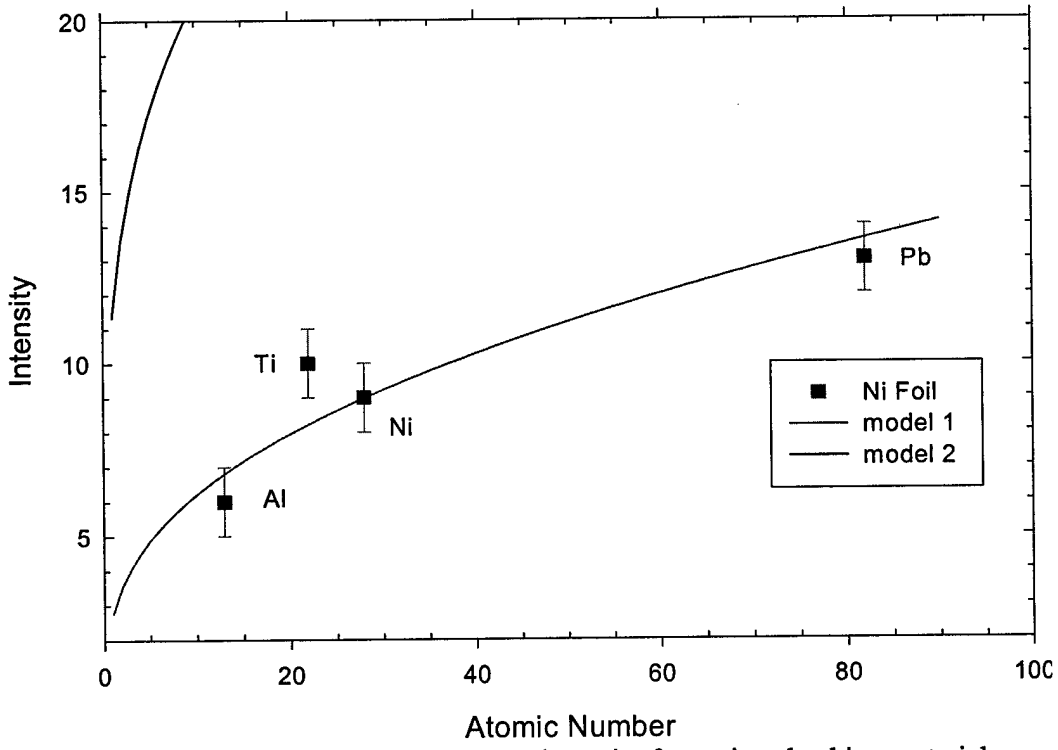

FIGURE 16 – Ni source foil component intensity for various backing materials

TABLE V – PALS results with correction for ^{22}NaCl contribution.

Metal	Source	1st Lifetime	2nd Lifetime	τ_B	χ^2
Al	Ni-1	145(1) ps 85(2) %	228(5) ps 14(2) %	153	1.079
Ti	Ni-1	134(1) ps 55(1) %	251(1) ps 44(1) %	169	1.101
Ni	Ni-1	104(4) ps 87(3) %	214(1) ps 13(1) %	112	1.100
Ta	Ni-1	131(2) ps 157(3) %	192(3) ps 42(3) %	151	1.230
Pb	Ni-1	178(1) ps 74(4) %	274(2) ps 42(2) %	174	1.13

TABLE VI – PALS results with correction for ^{22}NaCl and Ni source foil contribution

Metal	1st Lifetime	2nd Lifetime	χ^2	τ_B(expt)	τ_B
Al	153(1)ps 92(0.5) %	287(10)ps 11(2) %	1.104	157ps	160ps
Ti	140(1)ps 51(2) %	249(9) ps 49(3) %	1.07	178ps	146ps
Ni	104(1)ps 85(1) %	210(12)ps 15(2) %	1.104	112ps	102ps
Ta	133(2)ps 58(1) %	193(1)ps 42(1) %	1.24	153ps	116ps
Pb	183(1)ps 62(1) %	271(1)ps 38(1) %	1.14	203ps	200ps

The Ta fit shows a poor variance, the others are acceptable. The calculated bulk lifetimes are in reasonable agreement with previously reported values for Al, Ni and Pb. It is speculated that high, and varied, defect populations are present in the Ti and Ta samples which have not been correctly taken into account in the calculation of bulk lifetime.

PALS measurements on readily available polycrystalline pure metals have been performed. Fitting was performed with both MELT and Pattfit-88 has proved valuable, both have been found to give similar results. The number of lifetime components is determined by the fitting procedure used for MELT and provides insight on the likely number of resolved components. Pattfitt-88 allows source corrections to be conveniently applied. Controlling both programmes from within MATLAB has allowed laborious, systematic, variation of fitting parameters and screening of resulting outputs be performed very conveniently.

Clear evidence for the presence of source annihilations was found in the presence and nature of a third component in the fits and in the systematic variation in the calculated average lifetimes with source type. A long-lifetime source component was identified by systematically varying the lifetime and intensity of a fixed component and searching for minimum variance. The lifetime obtained of (430±10) ps is consistent with previous work. The variation in extracted intensity with Z of the material under study follows the expected trend. The method was also applied to identify a probably value for the source foil component. This gave values in the range range 110 – 120 ps for nickel and 230 – 240 ps for the aluminum source.

The variation in the intensity of the nickel source foil contribution with Z of the backing material was determined and found to be consistent with that calculated assuming a simple exponential implantation profile. The modified exponential model gave intensity values significantly greater than the experiment.

The lifetime components obtained from the data taken with a nickel-backed source allowed full source correction to be made. Bulk lifetime values were calculated from the corrected data. Poor agreement was found with other work for the Ti and Ta samples. These also showed high intensity defect components. The disagreement may result from competition between several populations of traps. In the case of Al, Ni, and Pb, the calculated bulk lifetimes were found to be in approximate agreement with previous work.

Preliminary PALS Study of Ceramic Pyroelectric Oxides

The main tasks achieved in this work plan were the construction and testing of a positron annihilation lifetime spectrometer and the development of careful methodologies to obtain reliable fitted positron lifetime values. The system was then used to study two pyroelectric material ceramics, a $(Pb,La)(Zr,Ti)O_3$ (PLZT) sample and a $Pb(Sc_{0.5},Ta_{0.5})O_3$ (PST) sample. The aim of these measurements was to determine if PALS was sensitive to vacancy defects in the ceramics as used in detector applications.

TABLE VII – PALS results on ceramic pyroelectric materials using MELT analysis

Sample	1st Lifetime	2nd Lifetime	χ^2
PST	225(4)ps 51(10) %	329(7)ps 40(10) %	1.004
PLZT	223(13)ps 52(9) %	338(22) ps 26(9) %	1.099

TABLE VIII – PALS results on ceramic pyroelectric materials using POSITRON and source correction

Sample	1st Lifetime	2nd Lifetime	χ^2
PST	223(2)ps 67(8) %	325(9) ps 33(12) %	1.104
PLZT	248(3)ps 72(12) %	343(7) ps 28(11) %	1.011

The results from the two ceramic oxide samples are shown in Tables VII and VIII. The results obtained by free fitting using maximum entropy methods are given in the former and those including source correction obtained using non-linear least squares are given in the latter. Both samples could be fitted satisfactory with a two-component model. The results for these two Pb based perovskite oxides are similar, a τ_1 in the 220-250 ps range and a longer vacancy defect lifetime, τ_2, in the 330-340 ps range.

This preliminary study has shown that PALS is sensitive to vacancy defects in these oxides. Further work on systematic sets of samples must follow.

EPR Studies of $Pb(Zr,Ti)O_3$ Materials

Electron paramagnetic resonance (EPR) is another powerful method allowing defects and impurities in ferroelectric materials to be identified and estimates of concentration made. Previous work on Mn doped $PbTiO_3$ has been detailed (N68171-98-M5740). These studies were made using single crystal material as may EPR spectra of interest are anisotropic, this information is required to make an unambiguous identification of the centre responsible. Here preliminary measurements on powder ceramic PZT materials are reported. The samples studied were doped with Mn, see Fig. 17.

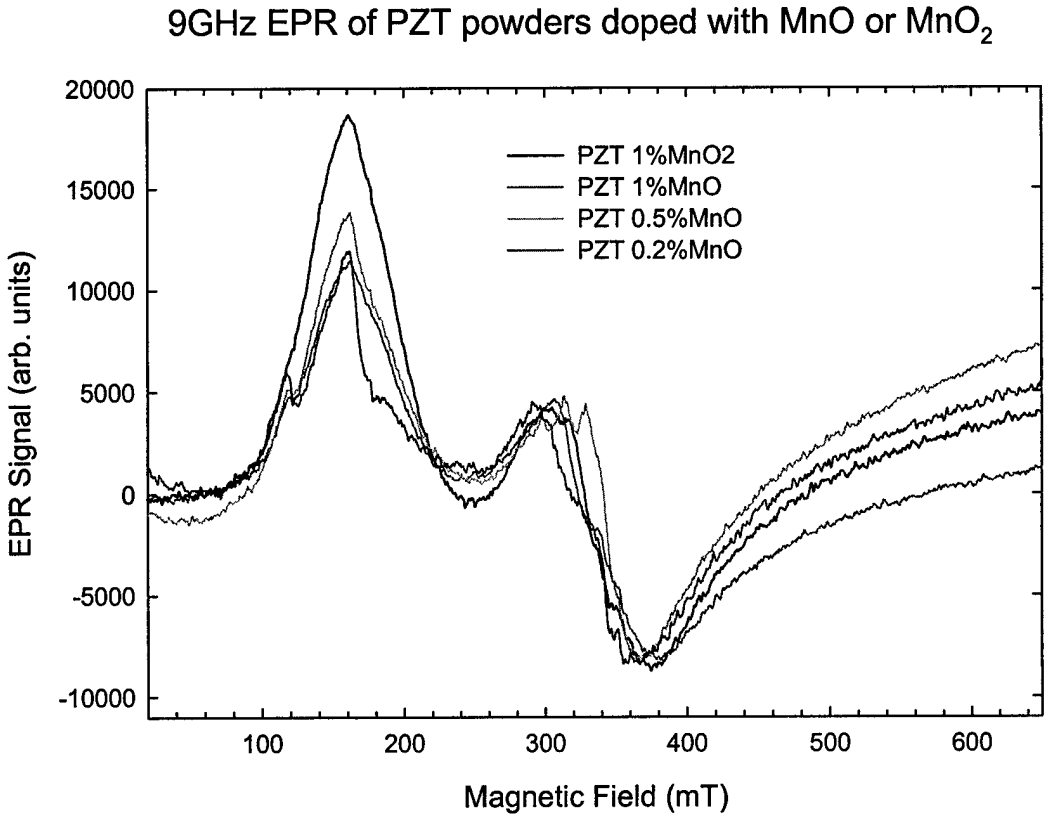

FIGURE 17 – 9GHz EPR spectra from $Pb(Zr,Ti)O_3$ powders doped with Mn using MnO or MnO_2.

A broad characteristic spectrum was recorded from each of the Mn doped powders. The spectra differed in terms of the relative intensities of the broad features at approximately 150 and 350 mT and in the linewidths and the presence of partially resolved structure. From previous single studies the low field feature can be mainly attributed to Mn^{4+} while the intensity in the region of 350 mT is likely due to Mn^{2+}. Manganese was introduced either using MnO_2 or MnO. As expected the intensity of the relative contribution of the Mn^{4+} component is greater for the sample doped using MnO_2.

Further work is in progress to study the spectra in more detail and to simulate the spectra based on appropriate spin-Hamiltonians. The double integrated area of the spectra are proportional to concentration, determining areas from these broad spectra, however, is difficult to do.

Concluding Remarks

An operational positron annihilation lifetime spectrometer has been constructed and tested. The resolution function width of approximately 205 ps with a count rate of 130 counts s^{-1} from a 370 kBq^{-1} source was achieved. Two independent analysis algorithms were tested using simulated lifetime spectra. Systematic studies were performed on a series of polycrystalline pure metal samples. This work confirmed the need for accurate source annihilation correction and allowed a methodology to be developed. Further, this procedure allowed the variation in backscatter source contribution with atomic number to be studied.

The spectrometer was then used to study two pyroelectric Pb based perovskite oxide ceramic samples, a La doped PZT sample, $(Pb,La)(Zr,Ti)O_3$, and an undoped $Pb(Sc_{0.5},Ta_{0.5})O_3$ (PST) sample. Fits using maximum entropy method and source corrected fitting using non-linear least square where found to be similar. A second vacancy defect contribution was clearly observed in both samples.

Electron paramagnetic resonance measurements were extended from earlier single crystal $PbTiO_3$ work to powder $Pb(Zr,Ti)O_3$ samples. A series of Mn doped samples was studied. The spectrum was found to contain contributions from both Mn^{4+} and Mn^{2+} charge states.

Literature cited

1. R.W. Whatmore, *Reports On Progress In Physics*, **49**(12), 1335 (1986).
2. D. Damjanovic, *Reports in the Progress of Physics*, **61**, 1267 (1998).
3. S. Pöykkö and D.J. Chadi, *Physical Review Letters*, **submitted** (1999).
4. W.L. Warren, C.H. Seager, D. Dimos, and E.J. Friebele, *Applied Physics Letters*, **61**(21), 2530 (1992).
5. W.L. Warren, B.A. Tuttle, *et al.*, *Materials Research Society Symposium*, **310**, 391 (1992).
6. W.L. Warren, B.A. Tuttle, *et al.*, *Applied Physics Letters*, **62**(5), 482 (1993).
7. W.L. Warren, B.A. Tuttle, *et al.*, *Applied Physics Letters*, **62**(2), 146 (1993).
8. W.L. Warren, D. Dimos, *et al.*, *Applied Physics Letters*, **65**(8), 1018 (1994).
9. D.J. Keeble, A. Krishnan, *et al.*, *Integr. Ferroelectr.*, **8**(1-2), 121 (1995).
10. D.J. Keeble, A. Krishnan, *et al.*, *Applied Physics Letters*, **73**(4), 508 (1998).
11. D.J. Keeble, B. Nielsen, *et al.*, *Applied Physics Letters*, **73**(3), 318 (1998).
12. T. Friessnegg, B. Nielsen, *et al.*, in *Ferroelectric Thin Films Viii*. 2000. p. 393.
13. T. Friessnegg, S. Aggarwal, *et al.*, *IEEE Trans. Ultrason. Ferroelectr. Freq. Control*, **47**(4), 916 (2000).
14. T. Friessnegg, S. Aggarwal, *et al.*, *Applied Physics Letters*, **77**(1), 127 (2000).
15. A. Shukla, M. Peter, and L. Hoffmann, *Nucl. Instrum. Methods Phys. Res. Sect. A-Accel. Spectrom. Dect. Assoc. Equip.*, **335**(1-2), 310 (1993).
16. P. Kirkegaard, M. Eldrup, and J.H. Evans, *Journal of Physics F-Metal Physics*, **6**, 499 (1976).
17. M. Iwami, E. Hashimoto, and Y. Ueda, *Journal of Physics-Condensed Matter*, **7**(50), 9935 (1995).
18. T. Korhonen, M.J. Puska, and R.M. Nieminen, *Phys. Rev. B*, **54**(21), 15016 (1996).
19. A. Seeger and F. Banhart, *Phys. Status Solidi A-Appl. Res.*, **102**(1), 171 (1987).
20. J.M. Campillo, F. Plazaola, and M.J. Puska, *Phys. Status Solidi B-Basic Res.*, **206**(2), 509 (1998).
21. T.E.M. Staab, R. KrauseRehberg, and B. Kieback, *Journal of Materials Science*, **34**(16), 3833 (1999).
22. M.J. Puska, *Journal of Physics-Condensed Matter*, **3**(20), 3455 (1991).
23. T.E.M. Staab, B. Somieski, and R. KrauseRehberg, *Nucl. Instrum. Methods Phys. Res. Sect. A-Accel. Spectrom. Dect. Assoc. Equip.*, **381**(1), 141 (1996).

Dissemination of Results

Publications
Papers with acknowledgement to N68171-99-M-6463

T. Friessnegg, B. Nielsen, and D.J. Keeble, "*Detection of oxygen vacancies in (Pb,La)(Zr,Ti)O_3 thin film capacitors using positron annihilation*", Integrated Ferroelectrics, **32**(1-4), 871-889 (2001).

D.J. Keeble, A.O. Tooke, G.J. Gerardi and E.H. Poindexter, *"Local structure anomaly in $PbTiO_3$ at low temperature studied by Mn^{4+} electron paramagnetic resonance"*, Physical Review B, **in preparation**

D.J. Keeble and M. Loyo-Menoyo, "*Electron paramagnetic resonance of Fe^{3+} in $PbTiO_3$*", Physical Review B, **in preparation**

S.McGuire and D.J. Keeble, "*Positron lifetime spectroscopy of polycrystalline metals*", Journal of Physics: Condensed Mater, **in preparation**